

# Stimulated-emission based model of fast radio bursts

Mustafa Doğan<sup>1</sup> and Kazım Yavuz Ekşi<sup>2</sup>

<sup>1</sup>*Istanbul Technical University, Faculty of Electrical-Electronics Engineering, Department of Control and Automation Engineering, 34469, Istanbul, Turkey, [mustafadogan@itu.edu.tr](mailto:mustafadogan@itu.edu.tr)*

<sup>2</sup>*Istanbul Technical University, Faculty of Science and Letters, Physics Engineering Department, 34469, Istanbul, Turkey, [eksi@itu.edu.tr](mailto:eksi@itu.edu.tr)*

11 March 2020

## ABSTRACT

Fast radio bursts (FRBs) are bright, short-duration radio transients with very high brightness temperatures implying highly coherent emission. We suggest that the FRBs are caused by the self-focusing of an electron beam interacting with an ambient plasma right beyond the light cylinder radius of a neutron star. The magnetic field at the light cylinder radius is relatively high which can accommodate both young Crab-like systems and old millisecond pulsars addressing the diverse environments of FRBs. At the first stage, the intense pulsed-beam passing through the background plasma causes instabilities such that the trapped particles in local Buneman-type cavitons saturate the local field. The beam is then radially self-focused due to the circular electric field developed by the two-stream instability which leads to Weibel instability in the transverse direction. Finally, the non-linear saturation of the Weibel instability results in the self-modulational formation of solitons due to plasmoid instability. The resonant solitary waves are the breather-type solitons hosting relativistic particles with self-excited oscillations. The analytical solutions obtained for non-linear dispersion and solitons suggest that, near the current sheets, the relativistic bunches are accelerated/amplified by klystron-like structures due to self-excited oscillations by the induced local electric field. Boosted coherent radio emission propagates through a narrow cone with strong focusing due to radial electric field and magnetic pinching. The non-linear evolution of solitons and the stimulated emission are associated with the Buneman instability and the possibility of the presence of nanosecond shots in FRBs are investigated.

**Key words:** instabilities: plasma - radiation mechanisms: general - magnetic fields: magnetic reconnection - stars: neutron

## 1 INTRODUCTION

Fast radio bursts (FRBs) are bright ( $\sim 0.1 - 1$  Jy) radio transients of duration  $\sim 0.1 - 10$  ms with very high brightness temperatures implying highly coherent emission (Lorimer et al. 2007; Thornton et al. 2013). Their dispersion measures (DM) being in excess of the Galactic contribution (Cordes & Lazio 2002), their isotropic distribution in the sky (Champion et al. 2016) as well as their recent localisation (Chatterjee et al. 2017; Bannister et al. 2019; Ravi et al. 2019) suggest they are cosmological sources (see Petroff et al. 2019; Cordes & Chatterjee 2019a, for reviews). To date  $\sim 10^2$  sources are detected at frequencies ranging between 400 MHz – 8 GHz (see Petroff et al. 2016, for a catalog of FRBs)<sup>1</sup>. FRBs have isotropic equivalent luminosities as high as  $\sim 10^{43}$  erg s<sup>-1</sup> and energies  $\sim 10^{40}$  ergs (Thornton et al. 2013). The most remarkable property of FRBs is the coherency of their emission as implied by their very high brightness temperatures  $T_B \gtrsim 10^{35}$  K.

Several exotic models such as cosmic strings (Yu et al. 2014;

Cao & Yu 2018), collisions between neutron stars and asteroids/comets (Geng & Huang 2015; Dai et al. 2016; Smallwood et al. 2019), mergers of charged black holes (Zhang 2016), axion quark nugget dark matter model (Van Waerbeke & Zhitnitsky 2019), black-to-white hole transition by non-perturbative quantum gravity effects (Barrau et al. 2018) and collapse of magnetospheres of Kerr-Newman black holes (Liu et al. 2016) have been proposed as the origin of FRBs (see Platts et al. 2018, for a catalog of theories). The detection of repeating FRB sources (Spitler et al. 2016; Scholz et al. 2016; CHIME/FRB Collaboration et al. 2019; The CHIME/FRB Collaboration et al. 2019; Kumar et al. 2019; Marcote et al. 2020; Fonseca et al. 2020), the deficiency of likely cataclysmic progenitors such as neutron star mergers (Falcke & Rezzolla 2014; Most et al. 2018) in supplying the occurrence rate of the FRBs per unit volume (Ravi et al. 2019) and population studies (Bhattacharya et al. 2019) suggest FRBs are non-catastrophic events. The detection of faint pulses from FRB 171019 (Kumar et al. 2019) implies that most FRBs repeat, even though they are undetected due to poor localisation.

Frequency drifts in FRBs point to neutron stars magnetospheres as the likely site for the origin of FRBs (Lyutikov 2019a,b).

<sup>1</sup> See the link <http://frbcat.org> associated with the paper.

Two of the likely models in this category are the magnetar model (Lyutikov 2002; Popov & Postnov 2010; Keane et al. 2012; Lyubarsky 2014; Pen & Connor 2015; Katz 2016; Wang & Yu 2017; Wang et al. 2018; Wadiasingh & Timokhin 2019; Cao et al. 2017; Beloborodov 2017, 2019; Maan et al. 2019) which suggests that FRBs are flares from young magnetars and the super-giant pulse model (Kulkarni et al. 2014; Cordes & Wasserman 2016; Connor et al. 2016; Popov & Pshirkov 2016; Lyutikov et al. 2016; Muñoz et al. 2019) which suggests that FRBs are extreme samples of giant pulses from younger-than-Crab rotationally powered pulsars.

The giant pulse model has the following advantages over the magnetar model:

(i) No radio emission was detected from SGR 1806-20 when it showed the magnetar giant flare (Tendulkar et al. 2016);

(ii) No FRBs were detected from the six gamma-ray burst remnants with possible magnetar engines (Men et al. 2019). The lack of high energy emission from FRBs is consistent with the lack of any enhancement in the high energy emission of Crab pulsar during giant pulses (Lundgren et al. 1995; Aliu et al. 2012; Bilous et al. 2012; Mickaliger et al. 2012; Hitomi Collaboration et al. 2018; MAGIC Collaboration et al. 2019). Detection of high energy emission contemporaneous with an FRB would strongly favour the magnetar model.

(iii) FRB 180814 (CHIME/FRB Collaboration et al. 2019) appears to show a 13 ms period Muñoz et al. (2019) within its sub-pulses which implies that FRB 180814 host a rotationally powered pulsar.

(iv) The pulse-energy distribution of the repeating FRB121102 (Spitler et al. 2014, 2016), is well described by a power law with index  $\alpha = -2.8 \pm 0.3$  (Gourdji et al. 2019), well in agreement with what Bera & Chengalur (2019) find for the Crab giant pulses (see also Argyle & Gower 1972; Majid et al. 2011; Mickaliger et al. 2012). Actually, this is not a very strong argument as the power-law nature of the amplitude distribution of bursts can be explained also by the magnetar model (Wang & Yu 2017).

(v) FRBs are localized to both star forming (high-metallicity) galaxies and low-metallicity ones suggesting that they can have both young and old central engines. As magnetars are preferentially young objects they can not address the localisation of some FRBs to low-metallicity environments. Giant pulses, on the other hand, are observed both from Crab-like young pulsars and recycled millisecond pulsars and are thus capable of addressing occurrence of FRBs in both environments.

There are problems also with the SGP model of FRBs: The instantaneous radio efficiency of SGPs as those seen in the Crab pulsar (Cordes et al. 2004) can reach values as high as  $\sim 10^{-2}$  (Cordes & Wasserman 2016; Lyutikov et al. 2016). Although this is well above the typical radio efficiency of pulsars,  $\sim 10^{-5}$ , it is still not enough to address the cosmological distribution as implied by both the dispersion measures and the redshifts, given the SGP models are limited by the spin-down power of young neutron stars. Indeed the SGP model initially was proposed as an extra-galactic but non-cosmological explanation for FRBs (Cordes & Wasserman 2016; Lyutikov & Lorimer 2016). Soon after the localisation of the repeating FRBs at  $\sim 1$  Gpc, Lyutikov (2017) argued that the measured cosmological distances exclude SGP model as the origin of FRBs (see also Meyers et al. 2017). Yet another well known issue is why more of the FRBs are not discovered from nearby galaxies but cosmological distances.

Note that FRBs must be emitted in low-density plasma as

$\nu \sim 1$  GHz radiation cannot propagate through plasma with  $n_e \sim 10^{10} \text{ cm}^{-3}$ . This introduces another limitation for the SGP model of FRBs since the central engines of FRBs, i.e. the rotationally powered pulsars, are then required to be older than 10 years, so that the supernova remnant (SNR) is transparent to GHz radio emission (Meyers et al. 2017; Bietenholz & Bartel 2019).

Recently, Machabeli et al. (2019) proposed a non-linear optical phenomenon, so called “self-trapping” (Chiao et al. 1964) as an intrinsic ingredient to any possible model to address the rare occurrence of FRBs and the luminosities observed. In this work, we suggest that FRBs are emitted from the current sheets right beyond the light cylinder radius of neutron stars (see §2) by the self-focusing electron beams composed of relativistic bunches with self-excited oscillations. For the first time to our knowledge we suggest that these oscillations are induced by breather-type solitons within the context of the stimulated emission providing the non-linear coherent radiation. The narrow beaming of the emission allows them to be observed from much larger distances with the inferred isotropic equivalent luminosities. We propose a model of two concentric cylinders where the outer one is the relatively slow ambient plasma and the inner one is the relativistic plasma jet<sup>2</sup>. The observed narrower pulse width of the emission corresponds to smaller beam opening angles (Zhang 2018). We find that FRBs consist of nanosecond shots such as seen in SGPs (Cordes et al. 2004); their angle of aperture thus can be as small as  $\theta \approx 3 \times 10^{-8}$  radians or the opening angle for the coherent emission can set the width of the beam. Our antenna-like maser emission model, proposed in the next section, is different from the maser emission models in the literature (Cordes & Chatterjee 2019b; Zhang 2018; Asseo et al. 1980; Plotnikov & Sironi 2019) in that we explain the population inversion dynamics. Finally, in §3 we discuss the implications of our model for FRBs.

## 2 A MECHANISM FOR FRBS

It is well established that the electric fields generated by a rotating neutron star is strong enough to extract charged particles from the surface of the star (Goldreich & Julian 1969). This forms a corotating plasma in the magnetosphere with density of the particles  $n_{\text{GJ}} \approx 7 \times 10^{10} B_{12}/P \text{ cm}^{-3}$  where  $B_{12}$  is the surface magnetic field in units of  $10^{12}$  G and  $P = 2\pi/\Omega$  is the rotation period of the pulsar (Goldreich & Julian 1969). The corotation of the particles is not possible beyond the light cylinder radius  $R_L \approx 5 \times 10^9 P \text{ cm}$  and accordingly the field lines crossing  $R_L$  open. The open field lines converge on the surface of the star to the polar caps with an opening angle  $\theta_p \approx \sqrt{R/R_L} \approx 0.014 P^{-1/2}$  rad. The secondary electron-positron pairs created by the  $\gamma$ -rays (Ruderman & Sutherland 1975) are accelerated along the open field lines emitting curvature radiation.

The dipole magnetic field of the neutron star declines with the radial distance  $r$  as  $B = \mu/r^3$  where  $\mu$  is the magnetic dipole moment. The magnetic field at the light cylinder radius,  $B_L = \mu/R_L^3$  is then

$$B_L = (2\pi)^3 \mu / c^3 P^3 \quad (1)$$

Assuming the neutron star is spinning down under magnetic dipole

<sup>2</sup> This is inspired by terrestrial maser production at room temperature (Breeze et al. 2018).

torques in a corotating plasma (Spitkovsky 2006)

$$I \frac{d\Omega}{dt} = -\frac{\mu^2 \Omega^3}{c^3} (1 + \sin^2 \alpha) \quad (2)$$

where  $I$  is the moment of inertia and  $\alpha$  is the inclination angle between rotation and magnetic axis. Solving the magnetic dipole moment from this equation we obtain

$$\mu = \frac{1}{2\pi} \sqrt{\frac{c^3 I}{1 + \sin^2 \alpha}} \sqrt{P \dot{P}} \quad (3)$$

Using Equation 3 in Equation 1 we find

$$B_L = (2\pi)^2 \sqrt{\frac{I \dot{P}}{c^3 P^5 (1 + \sin^2 \alpha)}} \approx 2 \times 10^8 \text{ G } \dot{P}^{1/2} P^{-5/2} \quad (4)$$

where we assumed  $I = 10^{45} \text{ g cm}^2$  and  $\alpha = 45^\circ$ .

The magnetic field at the light cylinder radius can be high ( $B_L \sim 2 - 3 \times 10^5 \text{ G}$ ) not only for Crab-like young neutron stars ( $P = 0.033 \text{ s}$ ,  $\dot{P} = 4.2 \times 10^{-13} \text{ s/s}$ ) but also for millisecond pulsars ( $P \sim 2 \times 10^{-3} \text{ s}$ ,  $\dot{P} \sim 10^{-20} \text{ s/s}$ ) which are old systems. Giant pulses tend to originate from pulsars with strong  $B_L$  (e.g. Wang et al. 2019) and are observed in millisecond pulsars as well as young Crab-like systems. The magnetar model of FRBs to date, however, can only address young systems<sup>3</sup>. We emphasise this point as FRBs are observed in diverse environments of both low-metallicity and high-metallicity (Marcote et al. 2020) indicating that they originate in both old and young systems. We note also that the period of a millisecond pulsar does not change as rapidly as a younger-than-Crab pulsar which implies systems that can live longer.

## 2.1 Early stages of the instability

The model we propose here is motivated by the plasma-beam systems in terrestrial experiments (see Figure 1). Plasma-beam systems have many applications in fusion reactors, astrophysics and plasma wake-fields for accelerating electrons to higher energies. These systems initially are both charge and current neutralised. The initial charge neutralisation implies the quasi-neutral property of plasma, while current neutralisation requires at least two streaming channels. Streams are often considered to be in opposite directions, but they can be parallel with opposite signs of currents. An intense pulsed-beam propagating through an ambient plasma leads to the development of streaming instabilities (Chen 2016). In nearly collisionless (low density) plasma, such instabilities based on kinetic behaviour of plasma, e.g. Buneman, two-stream, LHDI (lower hybrid drift instability) and Weibel, are known to cause particle trapping and acceleration in a relativistic setup (Krasovitskii 2008; Bret 2009; Chen 2016; Tokluoglu et al. 2018). At the initial stage, in plasma excited with a beam of bunched particles, the Buneman instability develops (Che et al. 2009). Galeev et al. (1981) proposed that, at the non-linear stage of the Buneman instability, short-lived non-stationary double layers or charge-separated regions will form by pinched electron currents due to strong longitudinal magnetic fields. At the boundaries of these regions, local electrons are accelerated excessively by the high electrical potential. The charge-separated regions thus become densely populated (Galeev et al.

1981). The trapping of the electrons by the Buneman instability leads to the growth of new instabilities, such as two-stream instability, following the non-linear saturation (Che et al. 2009). We require that the plasma density does not change smoothly at short distances so that the particles are decelerated and trapped in cavitons by the Buneman instability.

This saturation—or other possible ones due to sustained short duration oscillations, e.g. bouncing in small trap or caviton—can be disrupted by self-excited or triggered plasma events<sup>4</sup>. For example, the two-stream kinetic instability occurs when there are counter-streaming plasma flows in the velocity space in the presence of radiation pressure. The two-stream instability driven plasma can create a radial electric field, similar to the ponderomotive force dynamics (caviton formation, beam focusing, wave compression) (Tokluoglu et al. 2018). If the two-stream instability is excited, then the self-focusing of an electron beam moving through a plasma can be observed. This radial self-focusing is similar to a beam passing through a channel in a plasma. The radius of the beam, hence, diminishes in time while the local density of the particles increases uniformly (Krasovitskii 1969). The plasma, thus, acts as a non-linear medium for the focusing of the trapped particles (Machabeli et al. 2019). The efficiency of focusing increases at the relativistic regime (see § 3).

Following the two-stream instability, Weibel instability will develop in the transverse direction (Nishikawa et al. 2007). Weibel-like (filamentary) instabilities are known to be the underlying cause of the transverse field growth in a plasma (Chen 2016). The Weibel instability and the main electron acceleration are stimulated in the downstream region of electron-positron jets with plasma density perturbations leading to the formation of current filaments (Nishikawa et al. 2007). In the relativistic regime, the kinetic energy of these filaments is transferred to the magnetic field. The energy stored in the magnetic field is transferred partially back to the plasma particles due to saturation. The non-linear saturation developed at this stage is the origin of the induced electrostatic field which is responsible for the redistribution of particles along with the help of non-linearities, e.g. relativistic mass variation and ponderomotive force (Ghizzo 2013; Karsli et al. 2019; Farina & Bulanov 2005).

## 2.2 Non-linear evolution of the solitons and population inversion

The Weibel instability is an electromagnetic instability, that arises from plasma anisotropy. The Weibel instability generates a magnetic field which is perpendicular to the direction of the anisotropy which is reduced by axial momentum transfer. In a thin current sheet, seed-X-points are generated by the Weibel instability. The inner current region decays into a “magnetic vortex street” consisting of plasmoids and seed-X points (Tremann et al. 2010; Comisso et al. 2017). The importance of the plasmoid instability in actuating fast reconnection and fast energy transfer has recently gained attention (see Kagan et al. 2015, for a review). The role of plasmoids in the pulsar emission mechanism has recently been estab-

<sup>3</sup> Of course a short lived magnetar can form in old systems by merger of two neutron stars. These are associated with short gamma-ray bursts. Such a progenitor can not be associated with FRBs given that their rate of occurrence is much lower than FRBs and obviously that such a onetime process can not address repeating FRBs.

<sup>4</sup> Such that the growth of the Buneman instability is assisted by the self-excitation for sufficiently small time cycles (Galeev et al. 1981) and likewise plasma triggering is observed in microwave pulse compressors built to obtain narrow high peak pulses (Karsli et al. 2019). The following plasma behaviour such as new matched oscillations can result in higher amplitude pulse formation.

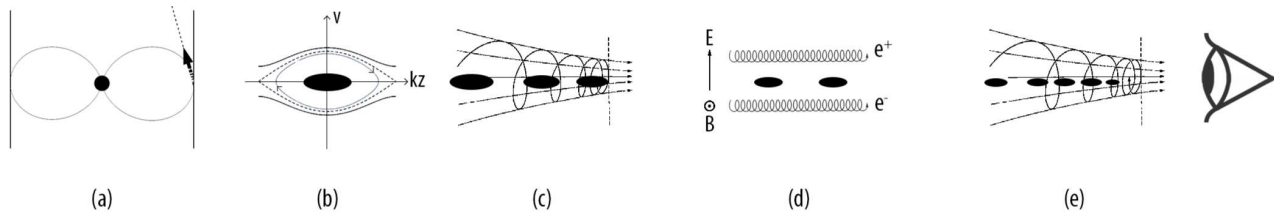


**Figure 1.** Illustration of the steps of the proposed mechanism: (a) the neutron star (the solid circle at the center) and its magnetosphere bounded by its light cylinder (the vertical solid line), seeding the coherent radiation (in the direction of arrow); (b) the creation of the bunched beam, within the trapping region, by the Buneman instability in phase space; (c) the mirroring, acceleration and focusing region by the two-stream instability with radial electric and non-uniform magnetic fields; (d) the bunched beam gains more kinetic energy by  $\mathbf{E} \times \mathbf{B}$  drift; (e) the focusing and boosting of the coherent emission as maser by velocity modulation along the line of sight.

lished (Cerutti & Philippov 2017; Philippov et al. 2019; Lyubarsky 2019). The plasmoid instability can be explained in terms of a tearing instability occurring in a reconnecting current sheet. This tearing process will force the inner current sheet to decay into a chain of highly dynamical magnetic islands with meso-scale plasmoids (Treumann et al. 2010; Comisso et al. 2017). These plasmoids can be depicted by the thin magnetic braids in the central part of the current sheet (Treumann et al. 2010; Comisso et al. 2017; Zenitani & Hesse 2008).

The plasma, when a powerful electromagnetic wave propagates within, acts as a non-linear medium. The high amplitude wave leads to the anisotropy of the medium resulting in further enhancement of the electric field and hence to the growth of the refraction index which is the origin of the non-linear dispersion (Machabelli et al. 2019). As the plasma wave is non-linear the ponderomotive force of the plasma waves removes the background plasma. Then a local depression in density constitutes a caviton. Plasma waves trapped in this cavity then form an isolated structure called an envelope soliton (Chen 2016).

During the rearrangement of the magnetic field topology, plasmoid instability evolves into current sheets intermittently that have Langmuir plasmons. These high-frequency plasmons can form Langmuir solitons due to modulational instability (Li & Zhang 1997; Chen 2016). Solitons or solitary waves propagating in non-linear dispersive media “pass-through” one another without losing their identity (Zabusky & Kruskal 1965). Non-linear dispersion can cause compression/focusing or generation of solitons, unlike the linear case. The electrostatic fluctuations and scattering cause current disruption in the central region of the current sheet. The non-uniform current disruptions re-create the magnetic reconnection, namely merging the magnetic field lines (Arons 2011; Singh 2004). Thus, the magnetic coalescence at X-points results in the conversion of magnetic energy to kinetic energy and particle acceleration. The fastest acceleration during magnetic reconnection occurs at the initial catastrophic X-point collapse, with the reconnection of electric fields. During the X-point collapse, particles are accelerated by charge-starved excessive electric fields resulting in immediate arc-like discharges and pinched currents due to plasmoid instability (Lyutikov et al. 2016). The nature of the interaction between beam particles (bunched together) and electromagnetic field while the interaction (energy-exchange) is significantly enhanced by the relativistic regime, explains the conditions for the existence of resonant solitons in non-equilibrium plasma beam systems. The energy density of the resonant electromagnetic solitons in non-equilibrium dispersive media is preserved (Bachin & Krasovitskii 1980).

To understand the coherent microwave emission, antenna-like maser mechanism with resonant peaks (Cordes & Chatter-

jee 2019b; Zhang 2018; Asseo et al. 1980; Plotnikov & Sironi 2019) with non-monotonic charge distribution due to electromagnetic trapping in plasma should be considered. Assuming plasma creation is dominated by the pair production caused by high energy photons, electron and positron densities can be similar. In our model, the self-excited maser mechanism can be explained such that the inner cylinder, as the magnetic mirror/bottle bounded by circular electric fields, is surrounded by ambient plasma which has non-uniform magnetic field. Here the inner cylinder represents the sapphire cavity and the outer one represents the copper cavity in terrestrial maser setup (Breeze et al. 2018). To grasp the coherence of the emission, klystron working principles can be summarised as follows: After the bunching of the electrons by the induced electric field, the bunches drifting by  $\mathbf{E} \times \mathbf{B}$ , rather than the thermal one, gain more energy for a while; the high kinetic energy of the bunches is then transferred to the electromagnetic wave by magnetic coupling or reconnection (see Figure 1). This charge separation due to radiation pressure (longitudinal electric fields with the strong external magnetic field) causes the non-linear saturation of the field amplitude similar to kinetic instabilities, e.g. the inherited Buneman, two-stream and Weibel instabilities in the current sheets (Arons 2011; Singh 2004).

The large amplitude electromagnetic pulses propagating in a plasma along a strong magnetic field under cyclotron resonance conditions are shown to take the form of solitons (Krasovitskii 2008, §5.5). The auto-resonance of solitons is then developed by the acceleration of the electrons to ultra-relativistic speeds suppressing the cyclotron resonance. Consequently, the coherent emission should be concentrated in a narrow hollow cone in the vicinity of the current sheets’ boundary. The cone must be hollow since the radiation is generated only near the current sheets, thus tracking the last open field lines (LOFL). The cone must be narrow because the opening angle is set by the nearly vertical directions of the LOFL above the polar caps (Zhang 2018). The observed radio signals from pulsars are quite narrow in time. For example, the first pulsar discovered, PSR B1919+21, has a period of 1.34 s but a pulse width of only around 40 ms which translates into a beam opening angle of one-tenth of the pulsar inclination angle (Zhang 2018).

The non-linear envelope solitons as self-modulational instability (caused by relativistic mass variation and ponderomotive dynamics) of pulsar micro-structures as proposed by Chian & Kennel (1983) are stable against longitudinal perturbations and mutual collisions. The intermittent and quasi-periodic nature of the observed pulsar micro-structures/pulses can be explained by the collection of envelope solitons with randomly fluctuating amplitudes (intermittency) or the latter (quasi-periodicity), a sequence of envelope soli-

tons with little variation in their peak amplitudes (Chian & Kennel 1983). Since a two-level system is usually unstable in the presence of small electromagnetic perturbations, a coherent emission of an electromagnetic wave is indispensable due to population inversion phenomena among the levels, such as maser mechanism. Because, the ambient plasma and current sheets are free from crystal structures similar to the diamond core in terrestrial maser setup (Breeze et al. 2018), we need to explain the population inversion mechanism in the current sheets. Buneman instability in current sheets results in bunching, magnetic reconnection, bifurcation of streams (Singh 2004). The relativistic bunches are decelerated and trapped in cavitons as small resonators. Along with this process an electron velocity gap (the trapping width) of magnitude

$$v_{\text{tr}} = \sqrt{\frac{2eE}{m_e k}} \propto \frac{\omega_b}{k}, \quad (5)$$

is developed (Dieckmann et al. 2000; Chen 1987). Here  $-e$  is the electron charge,  $E$  is the amplitude of electric field at which the Buneman wave traps a significant fraction of the electron population,  $m_e$  is electron rest mass,  $k$  is the wave-number and  $\omega_b$  is the bouncing frequency. During the evolution of the Buneman instability, the motion of the particles, governed by harmonic oscillator dynamics with bouncing frequency  $\omega_b$ , is trapped in a travelling wave. On the other hand, the bounce-time  $\propto \omega_b^{-1}$  for the trapped-particles is increased by the lower bouncing frequency associated with the diminished amplitude in the phase space for trapping (see Figure 1). For lower velocity electrons which have almost zero velocity at the boundary (separatrix) of the trapped region, the trapped fraction ( $n_{\text{tr}}$ , trapped density divided by the electron density,  $n_e$ ) of the population is given by (Dieckmann et al. 2000; Chen 1987)

$$\frac{n_{\text{tr}}}{n_e} = \frac{1}{\sqrt{2\pi}} \int_{v_p - v_{\text{tr}}}^{v_p + v_{\text{tr}}} e^{-v^2/v_e^2} dv. \quad (6)$$

Here  $v_p$  is phase velocity of the wave, and  $v_e \cong v_p - v_{\text{tr}}$  where large numbers of electrons are trapped (Dieckmann et al. 2000). Note that, the trapped fraction is exponentially sensitive to the magnitude of the electric field which is rapidly evolving in time. The population of the trapped/low-velocity electrons which can be represented as ground state carriers is increased by the population inversion followed by the stimulated emission. After being excited by the dense-beam, this population inversion is destroyed by the high-velocity bunches accelerated at the boundary as a precursor of the two-stream instability. Thus, the field-dependent trapped fraction of the population evolves in time to provide coherent stimulated emission. By this instability, broadened/enhanced electron velocity distribution (plateau-like distribution or double-humped electron distribution (Chen 2016)) establishes the oscillations in the phase space. Finally, the population inversion is achieved repeatedly around the quasi-equilibrium point of the bunch momentum (Zheleznyakov et al. 2001). These cavitons are re-filled up continuously following the energy interchange between the particles and the coherent electromagnetic waves. This phenomenon of the continuous passage of plasma through the cavitons guarantees that the population inversion is kept steady (Plotnikov & Sironi 2019; Chen 2016).

### 2.3 Non-linear two-level system

The resonant solitary waves in a non-linear two-level system (Krasovitskii 2008) have governing equations and solutions similar those given in Chian & Kennel (1983) (see also Leblond 2019;

Sazonov 2018; Pakula 2016). Resonant solitons are the breather-type solitons such as those observed in non-linear optical medium (Krasovitskii 2008; Leblond 2019). The non-linear dispersion law and the shape of the envelope solitons are governed by the following non-linear equations (see Krasovitskii 2008, §5.5):

$$\frac{\partial^2 \mathbf{E}}{\partial z^2} - \frac{1}{c^2} \frac{\partial^2 \mathbf{E}}{\partial t^2} = \frac{4\pi}{c^2} \frac{\partial^2 \mathbf{P}}{\partial t^2} \quad (7)$$

$$\frac{\partial^2 \mathbf{E}}{\partial t^2} + \omega_p^2 \mathbf{P} = -\frac{2Nd_0^2 \omega_p}{\hbar} W \mathbf{E} \quad (8)$$

where  $\mathbf{E}$  and  $\mathbf{P}$  are the electric field and polarisation vectors,  $c$  is the speed of light,  $\omega_p$  is the natural frequency of the medium (ambient plasma),  $N$  is the particle density and  $d_0$  is the dipole moment of separated charges within the Debye volume filled with aligned dipoles (Machabeli et al. 2019), and the population difference for the two levels is given by (Krasovitskii & Kurilko 1965)

$$W = -\sqrt{1 - \left(\frac{P}{Nd_0}\right)^2 - \left(\frac{1}{Nd_0\omega_p} \frac{\partial P}{\partial t}\right)^2}. \quad (9)$$

(see Appendix A). In the linear approximation to the governing equations, the electromagnetic waves that have harmonics at  $\exp(i\omega t - ikz)$  ( $i \equiv \sqrt{-1}$ ) have the following dispersion equation:

$$n_0^2(\omega) \equiv \left(\frac{ck}{\omega}\right)^2 = 1 + \frac{q^2}{\delta}, \quad \text{linear limit} \quad (10)$$

where  $\delta$  is the relativity parameter and  $q$  is the energy quantisation parameter given as

$$\delta \equiv \frac{\omega_p^2}{\omega^2} - 1, \quad q^2 \equiv \frac{8\pi Nd_0^2}{\hbar\omega_p}. \quad (11)$$

Here  $\hbar\omega_p$  is unit value of energy quantisation for the incident photons. The parameters above should satisfy the conditions

$$q^2 \ll 1, \quad |\delta| \ll 1, \quad |n^2 - 1| \ll 1. \quad (12)$$

for the existence of the soliton (see Appendix B). Note that as the number of cycles per oscillatory peak amplitude increases, attained at the limit of  $q^2/\delta^2 \rightarrow 1$ , the solitary wave complies better with the quasi-periodic structures observed in micro-pulses of giant pulses (Cordes 1979). On the other hand,  $\delta \rightarrow 0$  should be satisfied for the matched resonance and steady population inversion as well (Krasovitskii 2008). Thus, the above existence conditions for the solitary wave are met properly. Here, the strong non-linear coupling results in velocity modulation. Accordingly, the non-linear dispersion law obtained analytically without any approximation is

$$n^2(\omega) = 1 + \frac{q^2}{\delta} \left[ 1 + \left(\frac{q^2 \mathcal{E}_m}{8\pi\delta}\right)^2 \right]^{-1}, \quad \text{nonlinear, implicit} \quad (13)$$

(see §5.6 Krasovitskii 2008, or Appendix B below) where  $n(\omega)$  depends on  $\mathcal{E}_m$  which is the maximum field amplitude of the soliton,  $\mathcal{E}$ . The electromagnetic non-linearity is proportional to  $|n^2 - 1|$ . In a more explicit way, we can rewrite the above expression for the dispersion diagram (see Figure 2) for magnetized plasma with suppressed cyclotron resonance as:

$$n^2 - 1 = \frac{n_0^2 - 1}{1 + (n_0^2 - 1)^2 (\mathcal{E}_m/8\pi)^2}, \quad \text{nonlin w/o cyc} \quad (14)$$

where  $n_0 = ck/\omega$ . Here, the compression/focusing effect of the nonlinear dispersion,  $\propto \omega^{-6}$  implies a very narrow frequency bandwidth. For a resonant soliton with appropriate existence conditions,

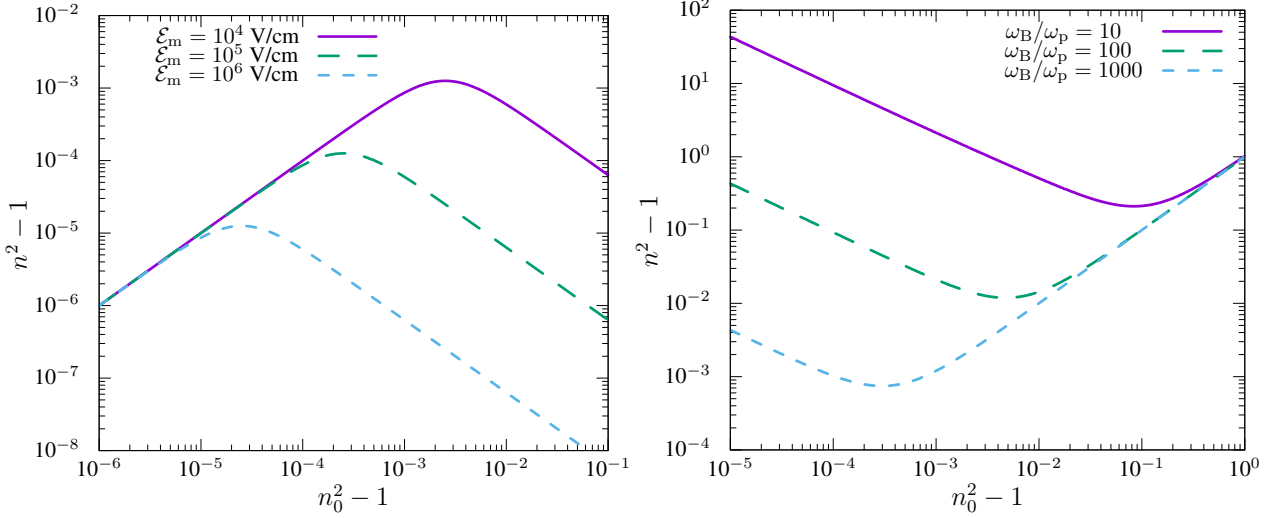


**Figure 2.** The electromagnetic non-linearity ( $n^2 - 1$ ) as a function of  $n_0^2 - 1$ . The left panel is for the case without cyclotron resonance (auto) given in Equation 14 and the right panel is for the case with cyclotron resonance given in Equation 17.

the analytical solutions for the group and phase velocities, and the breather-type soliton are as follows:

$$v_g = c \left( 1 + \frac{8N\hbar\omega_p}{E_m^2} \right)^{-1}, \quad v_p = c \quad (15)$$

$$\mathcal{E} = \mathcal{E}_m \operatorname{sech} \left[ \frac{d_0 E_m}{2\hbar} \left( t - \frac{z}{v_g} \right) \right] \quad (16)$$

(see §5.6 of Krasovitskii 2008, or Appendix B below) where  $E_m = Nd_0\mathcal{E}_m$  is the amplitude of the non-linear electric field  $E = Nd_0\operatorname{Re}(\mathcal{E})\exp(i\omega t - ikz)$ , for the envelope soliton. We emphasise that for solving the non-linear governing equations given in Equation 7 and Equation 8 we did not make any approximations or linearisations.

Assuming the presence of highly nonlinear cyclotron resonance and almost saturated electric field such that  $|\omega - \omega_B| \ll \omega_B$ , we can obtain the refraction index obeying the cyclotron resonance conditions (Krasovitskii 2008, §5.4) for the nonlinear system equations as follows

$$n^2(\omega) = n_0^2 + \frac{2\omega_p^2}{(\omega_B - \omega)^2 (n_0^2 - 1)^{2/3}}, \quad \text{nonlin w/ cyc} \quad (17)$$

where  $\omega_B$  is cyclotron frequency. Here,  $\omega_B$  can be set within the interval of 2 – 200 GHz (Lyutikov 2007) depending on relativistic mass, e.g. typical range of the Lorentz factor,  $\gamma = 5 - 500$  for mid-energetic electrons in pulsar magnetosphere (Cerutti et al. 2015). Finally, we observe that ignoring the nonlinear terms in the refraction index formulas, Equation 14 and Equation 17, will simplify to the known linear form (see e.g. Lyutikov 2007) as shown in Figure 2. The obtained solutions thus fully reflect the non-linear nature of the problem and is valid for the magnetized plasma in the relativistic regime right beyond the light cylinder radius.

### 3 DISCUSSION

In this work, we proposed a novel mechanism based on non-linear two-level system (Krasovitskii 2008) to address FRB phenomena. The model relies on the non-linear plasma processes near the light cylinder of a rotationally powered neutron star. The model can address the measured cosmological distances by showing that the

emission would be significantly beamed. Our principal result is that an astrophysical maser production mechanism feeds the klystron-like amplification of coherent emission. This is characterised by “self-excitation”, “self-focusing” and the highly coupled non-linear nature of the plasma medium. To produce a stable maser, the stimulated emission should be dominant over the excitation/absorption phenomena. For the relativistic bunches, the bounce-time for the trapped-particles,  $\propto \omega_b^{-1}$ , increases with the relativistic mass (see equation Equation 5 and § 2.2). Thus, a higher rate of beam-to-wave energy transfer is achieved with increased efficiency. Hence, the prevailing stimulated emission is succeeded.

The Buneman instability produces strong electron acceleration in highly magnetised plasma where a broad range of velocity distribution is provided. The quench time (including the growth and the saturation regimes) of the Buneman instability can be approximated as  $t_q \approx 40\pi/\omega_p$  where  $\omega_p$  is the electron plasma frequency (Dieckmann et al. 2000). The length of the caviton induced by the relativistic beam can be estimated as approximately  $15\lambda_d$  where  $\lambda_d$  is the electron Debye length of the plasma (Vieyro et al. 2017). The parameters of ambient plasma around the current sheet (partially based on the parameters given in Zhang (2018)) are summarised in Table 1.

The variation of the caviton length with respect to change in the particle velocity from relativistic speed to  $v_e$  in Equation 6 is in the range of 0.093 cm to 31 cm comparable to the numeric results in Dieckmann et al. (2000). This spatial range corresponds to time interval of 3 ps to 1 ns as the caviton passage time ( $\approx t_q$ ). In the neighbourhood of the current sheets, the plasma frequency  $\omega_p$  is approximately in the tens to hundreds of gigahertz range which matches with the time interval in the preceding paragraph (Zhang 2018). On the other hand, the growth rate of the instability is  $\propto t_q^{-2}$  assisted by the self-excitation for sufficiently small time cycles (Galeev et al. 1981). Thus, a very short caviton passage time can be enough to produce excessive potentials observed in the ns shots of SGPs and probably existing in FRBs. To our knowledge, this is the first time the stimulated emission is associated with the Buneman instability and the relevance of these mechanisms for FRBs is discussed. The main novelty of this research, the breather-type solitons and non-linear two-level system (see § 2.3) are explained in the context of the stimulated emission to provide coherent radiation.

Parameter	Value
Bulk Electron density	$n_e = 10^{11} - 10^{14} \text{ cm}^{-3}$
Bunched Electron density	$n_b = 10^7 - 10^8 \text{ cm}^{-3}$
Temperature	$8 \times 10^6 \text{ K}$
Magnetic field	$B_L \sim 2 - 3 \times 10^5 \text{ G}$
Cyclotron frequency	$\omega_B < 840 \text{ GHz}$
Plasma frequency	$1 \text{ GHz} < \omega_p < 90 \text{ GHz}$

**Table 1.** Reference parameters of the plasma close to the current sheet.

In the meantime, the sensitivity to changes in wave frequency of the non-linear dispersion and the envelope soliton for electric field and polarization is very low compared with others; thus only the matching condition is required. Hence, the broadband frequency spectrum can be covered as long as they are matched by the self-excitation mechanism. The local oscillations of the breather-type soliton are usually characterized by short time duration, as short as a few cycles, residing in the traveling wave (Leblond 2019).

The observed narrower pulse width of the emission corresponds to smaller beam opening angles (Zhang 2018). By considering the relatively short time window ( $\sim 1 \text{ ns}$ ) of SGPs, the opening angle of the narrow cone for coherent emission or angle of aperture,  $\theta$ , could have a maximum value of  $\theta_{\text{max}} = 2^\circ$ , calculated as the one-tenth of the average pulsar inclination angle (Zhang 2018) where  $\theta \ll \theta_{\text{max}}/10^6$  radian due to very short-duration breather-type solitons complying with the numerical results (Asseo et al. 1980; Zhang 2018). In the relativistic environment, a highly focused beam can have a much narrower tubular form with slanted emission direction (Dyks 2017) that emphasises the “rare” probability to match the line of sight. Relativistic particle velocities and higher frequency waves produce much smaller beam-width similar to narrower pulse effect (Melrose & Yuen 2016; Lorimer & Kramer 2012; Zhang 2018). Consequently, the velocity modulation or self-modulation at the boundary of the light cylinder close to current sheets, forms electron bunches that pass through a cavity-like resonator. These relativistic bunches are then accelerated/amplified by klystron-like structures with the evolution of “rare” matched conditions, e.g. “self-excitation” of the natural resonance modes. Thus, robust microwave emission in wild ambient plasma can pass through the outer space as strongly focused in a very narrow conic region.

If our model is correct we can predict novel multi-beam geometry inspired by the helix beam suggested by Dyks (2017). To represent the breather-type solitons of the helical vibrations/oscillations, we can propose a multi-beam model such that they originate from a very narrow tubular source. Furthermore, this model will help to match the discontinuities/anomalies in the observations such as drifting, nulling or double notch (profile moding) due to the single pulse assumption (Dyks 2017; Basu et al. 2019).

The extreme plasma lensing reported by Main et al. (2018) for the galactic millisecond pulsar B1957+20 indicates that radio pulses can be strongly amplified by lensing in ambient plasma (see also Bilous et al. 2019, for the case of B1744-24A). The flux enhancement factors of up to 70–80 at specific frequencies by plasma lensing implies a possible similarity with the FRB phenomena (Main et al. 2018). If the  $16.35 \pm 0.18 \text{ d}$  periodicity observed from FRB 180916.J0158+65 (The CHIME/FRB Collabo-

ration et al. 2020) is the orbital period of a binary system with an active pulsar, then this FRB can be considered as an extreme case of strongly amplified pulses from the above mentioned galactic millisecond pulsars where giant pulses are lensed through the ambient plasma provided by the stellar wind during periastron passage. The mechanism we propose here does not exclude the plasma lensing, but exists whenever a strong pulse travels through the medium.

## APPENDIX A: COUPLING BETWEEN THE LINEAR APPROXIMATION AND THE NON-LINEAR POPULATION DYNAMICS

Here we want to show how the approximation of the Gaussian probability distribution for the trapped fraction in Equation 6

$$\frac{n_{\text{tr}}}{n_e} = \frac{1}{\sqrt{2\pi}} \int_{v_p - v_{\text{tr}}}^{v_p + v_{\text{tr}}} e^{-v^2/v_c^2} dv,$$

is equivalent to the differences of tangent hyperbolic functions

$$\frac{n_{\text{tr}}}{n_e} \approx K_1 \left( \tanh(v_p + v_{\text{tr}}) - \tanh(v_p - v_{\text{tr}}) \right) \quad (\text{A1})$$

where  $K_1$  is a constant, as used in literature. In Equation 9 the magnitude of the polarisation vector  $P$  can be approximated by its non-linear part (main envelope soliton)

$$P \approx K_2 \text{sech}(x) \quad (\text{A2})$$

where  $x \equiv (d_0 E_m / 2\hbar) (t - z/v_g)$  is the argument (field-dependent) for polarization and  $K_2$  is a constant. When this approximation is substituted in Equation 9, we obtain

$$W \approx K_2 \tanh^2(x). \quad (\text{A3})$$

We thus show the same envelope shape is valid for both the linear and non-linear part as the tangent hyperbolic function of field-dependent variables. This is sufficient for the proof of the approximation we used in population inversion dynamics in Equation 6 and Equation 9.

## APPENDIX B: DERIVATION OF THE NONLINEAR DISPERSION RELATION

In this section we sketch the derivation of the nonlinear dispersion relation given in Equation 13 from Equation 7 and Equation 8 as explained in §5.6 of Krasovitskii (2008). One seeks solutions of Equation 7 and Equation 8 of the form

$$E = Nd_0 \text{Re} \mathcal{E}(\xi) \exp(i\Phi), \quad (\text{B1})$$

$$P = Nd_0 \text{Re} \mathcal{A}(\xi) \exp(i\Phi) \quad (\text{B2})$$

where

$$\Phi \equiv \omega t - kz, \quad \xi \equiv \omega_p(z - ut) \quad (\text{B3})$$

(Krasovitskii & Kurilko 1965). These equations are nonlinear wave envelope equations. Here  $u$  is the wave velocity. After substituting the equations above into Equation 7 and Equation 8, and using the inequalities given in Equation 12 which allows one to ignore the second derivatives of the amplitudes we obtain the ordinary differential equations

$$2i(n - \beta)\mathcal{E}' + (n^2 - 1)\mathcal{E} = 4\pi\mathcal{A}, \quad (\text{B4})$$

$$-2i\beta\mathcal{A}' + \delta\mathcal{A} = \frac{q^2}{4\pi} \sqrt{1 - \mathcal{A}^2} \mathcal{E} \quad (\text{B5})$$

where  $\beta = u/c$ . If one eliminates  $\mathcal{A}$  from the differential equations one obtains the nonlinear equation for the amplitude of the dimensionless complex field

$$4\beta(n - \beta)\mathcal{E}'' + 2i\Psi\mathcal{E}' + \delta(n^2 - 1)\mathcal{E} = \left(\frac{q}{4\pi}\right)^2 \Lambda^{1/2}\mathcal{E}. \quad (\text{B6})$$

where

$$\Psi = \delta(n - \beta) - \beta(n^2 - 1) \quad (\text{B7})$$

and

$$\Lambda = 16\pi^2 - 4(n - \beta)^2|\mathcal{E}'|^2 - (n^2 - 1)^2|\mathcal{E}|^2 - 2i(n - \beta)(\mathcal{E}^*\mathcal{E}' - \mathcal{E}\mathcal{E}'^*) \quad (\text{B8})$$

where ‘\*’ denotes the complex conjugate. To simplify further we can assume  $\Psi = 0$  which implies

$$\beta = \frac{n}{1 + (n^2 - 1)/\delta} \quad (\text{B9})$$

and  $\mathcal{E}$  is real which corresponds to a wave with resonant group velocity. We now define

$$y \equiv \frac{\mathcal{E}}{4\pi}|n^2 - 1|^2, \quad Q \equiv \frac{q^2}{\delta(n^2 - 1)}, \quad \tau \equiv \frac{|\delta|}{2\beta}\xi \quad (\text{B10})$$

where  $\tau$  is the new time variable. These allow one to recast [Equation B6](#) as

$$y'' + y = Q\sqrt{1 - y^2 - y'^2} \quad (\text{B11})$$

where the primes denote derivatives with respect to  $\tau$ . A soliton solution satisfying  $Q > 1$  (recall  $Q \approx \delta/(n^2 - 1)$ ) is satisfied easily is

$$y = \frac{2}{Q}\sqrt{Q - 1}\operatorname{sech}(\sqrt{Q - 1}\tau) \quad (\text{B12})$$

which is equivalent to [Equation 13](#) and results with [Equation 16](#).

## ACKNOWLEDGEMENTS

KYE acknowledges support from TÜBİTAK with grant number 118F028.

## REFERENCES

- Aliu E., Archambault S., Arlen T., Aune T., Beilicke M., Benbow W., Bouvier A., Buckley J. H., Bugaev V., Byrum K., Cesarini A., Ciupik L., Collins-Hughes E., Connolly M. P., Cui W., 2012, *ApJ*, 760, 136
- Argyle E., Gower J. F. R., 1972, *ApJ*, 175, L89
- Arons J., 2011, *Astrophysics and Space Science Proceedings*, 21, 165
- Asseo E., Pellat R., Rosado M., 1980, *ApJ*, 239, 661
- Bachin I. V., Krasovitskii V. B., 1980, *Zhurnal Eksperimentalnoi i Teoreticheskoi Fiziki*, 79, 472
- Bannister K. W., Deller A. T., Phillips C., Macquart J. P., Prochaska J. X., Tejos N., Ryder S. D., Sadler E. M., Shannon R. M., 2019, *Science*, 365, 565
- Barrau A., Moulin F., Martineau K., 2018, *Phys. Rev. D*, 97, 066019
- Basu R., Paul A., Mitra D., 2019, *Monthly Notices of the Royal Astronomical Society*, 486, 52165230
- Beloborodov A. M., 2017, *ApJ*, 843, L26
- Beloborodov A. M., 2019, *arXiv e-prints*, p. arXiv:1908.07743
- Bera A., Chengalur J. N., 2019, *MNRAS*, 490, L12
- Bhattacharya M., Kumar P., Lorimer D., 2019, *arXiv e-prints*:1902.10225, p. arXiv:1902.10225
- Bietenholz M. F., Bartel N., 2019, *arXiv e-prints*, p. arXiv:1905.06690

- Bilou A. V., McLaughlin M. A., Kondratiev V. I., Ransom S. M., 2012, *ApJ*, 749, 24
- Bilou A. V., Ransom S. M., Demorest P., 2019, *ApJ*, 877, 125
- Breeze J. D., Salvadori E., Sathian J., Alford N. M., Kay C. W. M., 2018, *Nature*, 555, 493
- Bret A., 2009, *ApJ*, 699, 990
- Cao X.-F., Yu Y.-W., 2018, *Phys. Rev. D*, 97, 023022
- Cao X.-F., Yu Y.-W., Dai Z.-G., 2017, *ApJ*, 839, L20
- Cerutti B., Philippov A., Parfrey K., Spitkovsky A., 2015, *MNRAS*, 448, 606
- Cerutti B., Philippov A. A., 2017, *A&A*, 607, A134
- Champion D. J., Petroff E., Kramer M., Keith M. J., Bailes M., Barr E. D., Bates S. D., Bhat N. D. R., Burgay M., Burke-Spolaor S., Flynn C. M. L., Jameson A., Johnston S., Ng C., Levin L., 2016, *MNRAS*, 460, L30
- Chatterjee S., Law C. J., Wharton R. S., Burke-Spolaor S., Hessels J. W. T., Bower G. C., Cordes J. M., Tendulkar S. P., Bassa C. G., Demorest P., Butler B. J., Seymour A., Scholz P., 2017, *Nature*, 541, 58
- Che H., Drake J. F., Swisdak M., Yoon P. H., 2009, *PRL*, 102, 145004
- Chen F. F., 2016, *Introduction to Plasma Physics and Controlled Fusion*. Springer
- Chen L., 1987, *Waves and Instabilities in Plasmas*. World scientific
- Chian A. C. L., Kennel C. F., 1983, *ApSS*, 97, 9
- Chiao R. Y., Garmire E., Townes C. H., 1964, *PRL*, 13, 479
- CHIME/FRB Collaboration Amiri M., Bandura K., Bhardwaj M., Boubel P., Boyce M. M., Boyle P. J., Brar C., Burhanpurkar M., Cassanelli T., Chawla P., Cliche J. F., Cubranic D., Deng M., 2019, *Nature*, 566, 235
- Comisso L., Lingam M., Huang Y. M., Bhattacharjee A., 2017, *ApJ*, 850, 142
- Connor L., Sievers J., Pen U.-L., 2016, *MNRAS*, 458, L19
- Cordes J. M., 1979, *Space Science Reviews*, 24, 567
- Cordes J. M., Bhat N. D. R., Hankins T. H., McLaughlin M. A., Kern J., 2004, *ApJ*, 612, 375
- Cordes J. M., Chatterjee S., 2019a, *arXiv e-prints*, p. arXiv:1906.05878
- Cordes J. M., Chatterjee S., 2019b, *ARA&A*, 57, 417
- Cordes J. M., Lazio T. J. W., 2002, *arXiv e-prints-astro-ph/0207156*, pp astro-ph/0207156
- Cordes J. M., Wasserman I., 2016, *MNRAS*, 457, 232
- Dai Z. G., Wang J. S., Wu X. F., Huang Y. F., 2016, *ApJ*, 829, 27
- Dieckmann M. E., Ljung P., Ynnerman A., McClements K. G., 2000, *Physics of Plasmas*, 7, 5171
- Dyks J., 2017, *MNRAS*, 471, L131
- Falcke H., Rezzolla L., 2014, *A&A*, 562, A137
- Farina D., Bulanov S. V., 2005, *Plasma Physics and Controlled Fusion*, 47, A73
- Fonseca E., Andersen B. C., Bhardwaj M., Chawla P., Good D. C., Josephy A., Kaspi V. M., Masui K. W., Mckinven R., Michilli D., Pleunis Z., Shin K., 2020, *ApJsubmitted*, arXiv:2001.03595, p. arXiv:2001.03595
- Galeev A. A., Sagdeev R. Z., Shapiro V. D., Shevchenko V. I., 1981, *Zhurnal Eksperimentalnoi i Teoreticheskoi Fiziki*, 81, 572
- Geng J. J., Huang Y. F., 2015, *ApJ*, 809, 24
- Ghizzo A., 2013, *Physics of Plasmas*, 20, 082111
- Goldreich P., Julian W. H., 1969, *ApJ*, 157, 869
- Gourdji K., Michilli D., Spitler L. G., Hessels J. W. T., Seymour A., Cordes J. M., Chatterjee S., 2019, *ApJ*, 877, L19
- Hitomi Collaboration Aharonian F., Akamatsu H., Akimoto F., Allen S. W., Angelini L., Audard M., Awaki H., Axelsson M., Bamba A., Bautz M. W., Blandford R., Brenneman L. W., Brown G. V., Bulbul E., 2018, *PASJ*, 70, 15
- Kagan D., Sironi L., Cerutti B., Giannios D., 2015, *Space Science Reviews*, 191, 545
- Karsli O., Dogan M., Ahiska F., Orkun Sirel O., 2019, *IEEE Transactions on Plasma Science*, 47, 2823
- Katz J. I., 2016, *ApJ*, 826, 226
- Keane E. F., Stappers B. W., Kramer M., Lyne A. G., 2012, *MNRAS*, 425, L71
- Krasovitskii V. B., 1969, *Journal of Experimental and Theoretical Physics*, 29, 1252

- Krasovitskii V. B., 2008, Self-focusing of relativistic electron bunches in a plasma. Nova Science Publishers
- Krasovitskii V. B., Kurilko V. I., 1965, Soviet Journal of Experimental and Theoretical Physics, 21, 232
- Kulkarni S. R., Ofek E. O., Neill J. D., Zheng Z., Juric M., 2014, ApJ, 797, 70
- Kumar P., Shannon R. M., Osłowski S., Qiu H., Bhandari S., Farah W., Flynn C., Kerr M., Lorimer D. R., Macquart J. P., Ng C., Phillips C. J., Price D. C., Spiewak R., 2019, arXiv e-prints, p. arXiv:1908.10026
- Leblond H., 2019, Phys. Rev. A, 99, 053846
- Li X. Q., Zhang Z. D., 1997, ApJ, 479, 1028
- Liu T., Romero G. E., Liu M.-L., Li A., 2016, ApJ, 826, 82
- Lorimer D. R., Bailes M., McLaughlin M. A., Narkevic D. J., Crawford F., 2007, Science, 318, 777
- Lorimer D. R., Kramer M., 2012, Handbook of Pulsar Astronomy. Cambridge University Press
- Lundgren S. C., Cordes J. M., Ulmer M., Matz S. M., Lomatch S., Foster R. S., Hankins T., 1995, ApJ, 453, 433
- Lyubarsky Y., 2014, MNRAS, 442, L9
- Lyubarsky Y., 2019, MNRAS, 483, 1731
- Lyutikov M., 2002, ApJ, 580, L65
- Lyutikov M., 2007, MNRAS, 381, 1190
- Lyutikov M., 2017, ApJ, 838, L13
- Lyutikov M., 2019a, arXiv e-prints, p. arXiv:1908.07313
- Lyutikov M., 2019b, arXiv e-prints, p. arXiv:1909.10409
- Lyutikov M., Burzawa L., Popov S. B., 2016, MNRAS, 462, 941
- Lyutikov M., Lorimer D. R., 2016, ApJ, 824, L18
- Lyutikov M., Sironi L., Komissarov S., Porth O., 2016, arXiv e-prints, p. arXiv:1603.05731
- Maan Y., Joshi B. C., Surnis M. P., Bagchi M., Manoharan P. K., 2019, ApJ, 882, L9
- Machabeli G., Rogava A., Tevdorashvili B., 2019, MNRAS, 489, 5688
- MAGIC Collaboration Ahnen M. L., Ansoldi S., Antonelli L. A., Arcaro C., Babić A., Banerjee B., Bangale P., Barres de Almeida U., Barrio J. A., Becerra González J., Bednarek W., 2019, arXiv e-prints, p. arXiv:1911.00634
- Main R., Yang I. S., Chan V., Li D., Lin F. X., Mahajan N., Pen U.-L., Vanderlinde K., van Kerkwijk M. H., 2018, Nature, 557, 522
- Majid W. A., Naudet C. J., Lowe S. T., Kuiper T. B. H., 2011, ApJ, 741, 53
- Marcote B., Nimmo K., Hessels J. W. T., Tendulkar S. P., Bassa C. G., Paragi Z., Keimpema A., Bhardwaj M., Karuppusamy R., 2020, Nature, 577, 190
- Melrose D. B., Yuen R., 2016, Journal of Plasma Physics, 82, 635820202
- Men Y., Aggarwal K., Li Y., Palaniswamy D., Burke-Spolaor S., Lee K. J., Luo R., Demorest P., Tendulkar S., Agarwal D., Young O., Zhang B., 2019, arXiv e-prints, p. arXiv:1908.10222
- Meyers B. W., Tremblay S. E., Bhat N. D. R., Shannon R. M., Kirsten F., Sokolowski M., Tingay S. J., Oronsaye S. I., Ord S. M., 2017, ApJ, 851, 20
- Mickaliger M. B., McLaughlin M. A., Lorimer D. R., Langston G. I., Bilous A. V., Kondratiev V. I., Lyutikov M., Ransom S. M., Palliyaguru N., 2012, ApJ, 760, 64
- Most E. R., Nathanail A., Rezzolla L., 2018, ApJ, 864, 117
- Muñoz J. B., Ravi V., Loeb A., 2019, arXiv e-prints, p. arXiv:1909.00004
- Nishikawa K. I., Hededal C., Hardee P., Fishman G. J., Kouveliotou C., Mizuno Y., 2007, in Aschenbach B., Burwitz V., Hasinger G., Leibundgut B., eds, Relativistic Astrophysics Legacy and Cosmology - Einstein's Legacy Particle Acceleration with Weibel Instability. p. 462
- Pakula R. A., 2016, arXiv e-prints, p. arXiv:1612.00110
- Pen U.-L., Connor L., 2015, ApJ, 807, 179
- Petroff E., Barr E. D., Jameson A., Keane E. F., Bailes M., Kramer M., Morello V., Tabbara D., van Straten W., 2016, PASA, 33, e045
- Petroff E., Hessels J. W. T., Lorimer D. R., 2019, A&ARv, 27, 4
- Philippov A., Uzdensky D. A., Spitkovsky A., Cerutti B., 2019, ApJ, 876, L6
- Platts E., Weltman A., Walters A., Tendulkar S. P., Gordin J. E. B., Kandhai S., 2018, arXiv e-prints, p. arXiv:1810.05836
- Plotnikov I., Sironi L., 2019, MNRAS, 485, 3816
- Popov S. B., Postnov K. A., 2010, in Harutyunian H. A., Micaelaian A. M., Terzian Y., eds, Evolution of Cosmic Objects through their Physical Activity Hyperflares of SGRs as an engine for millisecond extragalactic radio bursts. pp 129–132
- Popov S. B., Pshirkov M. S., 2016, MNRAS, 462, L16
- Ravi V., Catha M., D'Addario L., Djorgovski S. G., Hallinan G., Hobbs R., Kocz J., Kulkarni S. R., Shi J., Vedantham H. K., Weinreb S., Woody D. P., 2019, Nature, 572, 352
- Ruderman M. A., Sutherland P. G., 1975, ApJ, 196, 51
- Sazonov S. V., 2018, in Journal of Physics Conference Series Vol. 1068, On the phase and group velocities of optical solitons. p. 012012
- Scholz P., Spitler L. G., Hessels J. W. T., Chatterjee S., Cordes J. M., Kaspi V. M., Wharton R. S., Bassa C. G., Bogdanov S., Camilo F., Crawford F., Deneva J., van Leeuwen J., 2016, ApJ, 833, 177
- Singh N., 2004, Nonlinear Processes in Geophysics, 11, 153
- Smallwood J. L., Martin R. G., Zhang B., 2019, MNRAS, 485, 1367
- Spitkovsky A., 2006, ApJ, 648, L51
- Spitler L. G., Cordes J. M., Hessels J. W. T., Lorimer D. R., McLaughlin M. A., Chatterjee S., Crawford F., Deneva J. S., Kaspi V. M., Wharton R. S., Allen B., Bogdanov S., Brazier A., 2014, ApJ, 790, 101
- Spitler L. G., Scholz P., Hessels J. W. T., Bogdanov S., Brazier A., Camilo F., Chatterjee S., Cordes J. M., Crawford F., Deneva J., Ferdman R. D., Freire P. C. C., Kaspi V. M., 2016, Nature, 531, 202
- Tendulkar S. P., Kaspi V. M., Patel C., 2016, ApJ, 827, 59
- The CHIME/FRB Collaboration : Andersen B. C., Bandura K., Bhardwaj M., Boubel P., Boyce M. M., Boyle P. J., Brar C., Cassanelli T., Chawla P., Cubranic D., Deng M., Dobbs M., Fandino M., 2019, arXiv e-prints, p. arXiv:1908.03507
- The CHIME/FRB Collaboration Amiri M., Andersen B. C., Bandura K. M., Bhardwaj M., Boyle P. J., Brar C., Chawla P., Chen T., Cliche J. F., Cubranic D., 2020, arXiv e-prints, p. arXiv:2001.10275
- Thornton D., Stappers B., Bailes M., Barsdell B., Bates S., Bhat N. D. R., Burgay M., Burke-Spolaor S., Champion D. J., Coster P., 2013, Science, 341, 53
- Tokluoglu E. K., Kaganovich I. D., Carlsson J. A., Hara K., Startsev E. A., 2018, Physics of Plasmas, 25, 052122
- Treumann R. A., Nakamura R., Baumjohann W., 2010, Annales Geophysicae, 28, 1935
- Van Waerbeke L., Zhitnitsky A., 2019, Phys. Rev. D, 99, 043535
- Vieyro F. L., Romero G. E., Bosch-Ramon V., Marcote B., del Valle M. V., 2017, A&A, 602, A64
- Wadiasingh Z., Timokhin A., 2019, ApJ, 879, 4
- Wang F. Y., Yu H., 2017, J. of Cosmology and Astroparticle Phys., 2017, 023
- Wang W., Lu J., Zhang S., Chen X., Luo R., Xu R., 2019, Science China Physics, Mechanics, and Astronomy, 62, 979511
- Wang W., Luo R., Yue H., Chen X., Lee K., Xu R., 2018, ApJ, 852, 140
- Yu Y.-W., Cheng K.-S., Shiu G., Tye H., 2014, J. of Cosmology and Astroparticle Phys., 2014, 040
- Zabusky N. J., Kruskal M. D., 1965, PRL, 15, 240
- Zenitani S., Hesse M., 2008, Physics of Plasmas, 15, 022101
- Zhang B., 2016, ApJ, 827, L31
- Zhang F., 2018, A&A, 612, A24
- Zheleznyakov V. V., Koryagin S. A., Thejappa G., 2001, Astronomical and Astrophysical Transactions, 20, 333